Title

Disruption of both nesprin 1 and desmin results in nuclear anchorage defects and fibrosis in skeletal muscle

Journal

Human Molecular Genetics, 23(22)

ISSN

0964-6906

Authors

Chapman, Mark A
Zhang, Jianlin
Banerjee, Indroneal
et al.

Publication Date

2014-11-15

DOI

10.1093/hmg/ddu310

Peer reviewed

Human Molecular Genetics, 2014, Vol. 23, No. 22 **5879–5892**
doi:10.1093/hmg/ddu310
Advance Access published on June 18, 2014

Disruption of both nesprin 1 and desmin results in nuclear anchorage defects and fibrosis in skeletal muscle

Mark A. Chapman[2,†], Jianlin Zhang[1,†], Indroneal Banerjee[1], Ling T. Guo[3], Zhiwei Zhang[5], G. Diane Shelton[3], Kunfu Ouyang[1,6], Richard L. Lieber[2,4] and Ju Chen[1,*]

[1]Department of Medicine, [2]Department of Bioengineering and [3]Department of Pathology, University of California San Diego, 9500 Gilman Drive, La Jolla, CA 92093, USA, [4]Department of Orthopaedic Surgery, University of California San Diego, and Department of Veteran's Affairs, 9500 Gilman Drive, La Jolla, CA 92093-0863, USA, [5]Department of Cardiothoracic Surgery, The Second Xiangya Hospital of Central South University, No. 139 Renmin Road, Changsha, Hunan 410011, P.R. China and [6]School of Chemical Biology and Biotechnology, Peking University, Shenzhen 518055, P.R. China

Received May 5, 2014; Revised June 9, 2014; Accepted June 16, 2014

Proper localization and anchorage of nuclei within skeletal muscle is critical for cellular function. Alterations in nuclear anchoring proteins modify a number of cellular functions including mechanotransduction, nuclear localization, chromatin positioning/compaction and overall organ function. In skeletal muscle, nesprin 1 and desmin are thought to link the nucleus to the cytoskeletal network. Thus, we hypothesize that both of these factors play a key role in skeletal muscle function. To examine this question, we utilized global ablation murine models of nesprin 1, desmin or both nesprin 1 and desmin. Herein, we have created the nesprin-desmin double-knockout (DKO) mouse, eliminating a major fraction of nuclear-cytoskeletal connections and enabling understanding of the importance of nuclear anchorage in skeletal muscle. Globally, DKO mice are marked by decreased lifespan, body weight and muscle strength. With regard to skeletal muscle, DKO myonuclear anchorage was dramatically decreased compared with wild-type, nesprin $1^{-/-}$ and desmin$^{-/-}$ mice. Additionally, nuclear-cytoskeletal strain transmission was decreased in DKO skeletal muscle. Finally, loss of nuclear anchorage in DKO mice coincided with a fibrotic response as indicated by increased collagen and extracellular matrix deposition and increased passive mechanical properties of muscle bundles. Overall, our data demonstrate that nesprin 1 and desmin serve redundant roles in nuclear anchorage and that the loss of nuclear anchorage in skeletal muscle results in a pathological response characterized by increased tissue fibrosis and mechanical stiffness.

INTRODUCTION

Skeletal muscle is a composite hierarchical tissue composed of myofibers embedded in extracellular matrix (ECM). At the myofibrillar level, actin and myosin, in combination with other proteins, comprise the sarcomere, the functional contractile unit in skeletal muscle (1). Structural proteins, such as dystrophin, interconnect myofibrils within a fiber to the ECM via the dystroglycan complex (DGC) (2). It is known that myopathies result when mutations occur in proteins associated with the DGC as well as in other structural proteins associated with the sarcolemma and organelles, such as the nucleus (2). In the present study, we probed the connections between the nucleus and the rest of the cell, to determine whether disruption of these connections leads to muscle defects.

Proper localization and anchorage of the nucleus within skeletal muscle is critical for cellular function (3–5). A number of recent studies demonstrated that loss of nuclear anchorage, localization and integration of mechanical signaling results in muscle defects (5–7). Recent attention has turned to protein

*To whom correspondence should be addressed. Tel: +1 8588224276; Fax: +1 8585342069; Email: juchen@ucsd.edu
†M.A.C and J.Z. contributed equally to this work.

complexes that link the nucleus to the cytoskeleton (3–5,8,9). These factors are necessary for mechanosensing, nuclear anchorage and positioning. Deficiencies in these connections have been associated with decreases in muscle function (5). Two factors, nesprin 1 and desmin, are of particular interest as they have been shown to play roles in anchorage, mechanical loading and localization of the nucleus (5,7). Moreover, these proteins are compromised in a number of murine and human pathologies, including Emery-Dreifuss Muscular Dystrophy (EDMD) (5,6,10–12). Thus, understanding the nuclear anchorage proteins nesprin 1 and desmin can lend deeper insight into the importance of nuclear anchorage in skeletal muscle.

Nesprins are a family of nuclear proteins that contribute to maintaining proper skeletal and cardiac muscle function as well as nuclear anchorage, positioning and morphology (5,6,11). Nesprins belong to a family of ubiquitously expressed type II transmembrane, spectrin-repeat proteins (Nesprin 1–4, KASH5) that anchor nuclei to actin filaments, intermediate filaments and the microtubule cytoskeleton (13). Nesprin 1 and 2 are highly expressed in skeletal muscle and produce a number of isoforms that vary markedly in size via alternative transcription initiation, RNA splicing or termination (13–16). Structurally, these factors link the actin cytoskeleton via two N-terminal calponin-homology domains and contain a variable number of spectrin repeats (14,15,17–19). Key to these factors is a conserved Klarsicht, ANC-1 and Syne C-terminal homology (KASH) domain (13). The KASH domain anchors nesprin 1 and 2 to the outer nuclear membrane (ONM) and links them to the inner nuclear membrane-binding partners, the SUN (Sad1p/UNC84) proteins. It has also been reported that nesprin 3 interacts with SUN proteins via its KASH domain and links to desmin via plectin (20,21).

Recent data from our laboratory showed that loss of nesprin 1 results in a mild dystrophic murine phenotype (5). This study demonstrated that nesprin 1 ablation results in skeletal muscle defects, reduced survival and altered nuclear position of myonuclei under basal conditions and in response to tensile loading (5). Moreover, this report demonstrated that removal of nesprin 1 resulted in partial, but not complete loss of nuclear anchorage. Thus, these data suggest that other proteins could play redundant roles in skeletal muscle nuclear anchorage.

Other proteins thought to interact with the nucleus, specifically desmin, could aid nesprin 1 in providing nuclear anchorage within skeletal muscle. Desmin primarily functions as the major intermediate filament in skeletal muscle. Desmin is responsible for linking adjacent myofibrils to one another and the sarcolemma (22). These interactions mechanically stabilize skeletal muscle and limit sarcomere length heterogeneities (7,23,24). Apart from structurally stabilizing myofibers, it has been shown that desmin is linked to the ONM protein nesprin 3 via plectin (21). Ablation of desmin has been linked to partial nuclear anchorage defects and altered nuclear deformation in skeletal muscle during passive fiber loading (7,25). Additionally, mutations in desmin alter disease severity in patients with EDMD, a dystrophy associated with mutations in nuclear-associated proteins (10).

Given that both nesprin 1 and desmin contribute to nuclear anchorage and positioning, we hypothesize that muscle nuclei are anchored to the cytoskeleton in two major ways: by interaction with the intermediate filament desmin through its connection with nesprin 3 and by interaction of nesprin 1 with actin myofilaments. Furthermore, we hypothesize that alterations in both connections will lead to more severe pathological phenotypes. To address this hypothesis, we developed a murine model where we globally ablated nesprin 1 (nesprin $1^{-/-}$), desmin (desmin$^{-/-}$) or both nesprin 1 and desmin (DKO). We found that dual ablation increased mortality and caused a more severe dystrophic phenotype. Interestingly, double-knockout (DKO) mice also had exacerbated nuclear defects (anchorage and positioning) as well as decreased nuclear deformation under tensile loading compared with control or single-knockout mice. We conclude that nesprin 1 and desmin play key and redundant roles in skeletal muscle nuclei anchorage and that loss of nuclear anchorage results in a dystrophic-like phenotype.

RESULTS

Ablation of both nesprin 1 and desmin results in increased mortality, decreased body weight and increased kyphosis

To examine the role(s) of nesprin 1 and desmin, we crossed our knockout lines for nesprin 1 (nesprin $1^{-/-}$) (5) and desmin (desmin$^{-/-}$) (22) to ablate both nesprin 1 and desmin (DKO) and examined the global phenotypes of these mice. Survival rates were examined in each of the four experimental groups. Both wild-type and desmin$^{-/-}$ lines presented with 100% survival at 13 months of age (Fig. 1A). Consistent with previous studies, ∼60% of nesprin $1^{-/-}$ animals died within 2 weeks of birth and these mice did not have increased mortality after this point. Interestingly, DKO mice had a similar (∼60%) decrease in survival during the first 2 weeks of life. However, unlike nesprin $1^{-/-}$ or desmin$^{-/-}$ mice, DKO mice survival continued to decline, with all mice dead after 13 months (Fig. 1A). In addition, DKO mice able to survive past 2 weeks had significantly decreased body weight compared with their wild-type, nesprin $1^{-/-}$ and desmin$^{-/-}$ controls (Fig. 1B).

DKO mice presented with indicators of exacerbated pathological phenotypes. At birth, wild-type, nesprin $1^{-/-}$, desmin$^{-/-}$ and DKO mice all presented with normal body shape and size. However, after weaning, DKO mice had impaired growth and kyphosis as determined by visual inspection and X ray (Fig. 2). These data indicate that loss of both nesprin 1 and desmin in DKO mice results in exacerbated development of pathological phenotypes compared with the other three experimental groups.

Strength and coordination are significantly decreased in double-knockout mice

Strength and coordination of 3- and 6-month-old mice were assessed by measuring forelimb grip strength and the ability to remain on a rotating rod (rotarod), respectively. At both 3 and 6 months of age, wild-type and nesprin $1^{-/-}$ animals had the highest peak force, both significantly higher than desmin$^{-/-}$ and DKO animals (Fig. 3A). DKO animals had the lowest maximum force at 3 and 6 months compared with the other three genotypes. To assess coordination, mice were placed on a rotarod and the amount of time they were able to stay on was recorded. At 3 months of age, wild-type and nesprin $1^{-/-}$

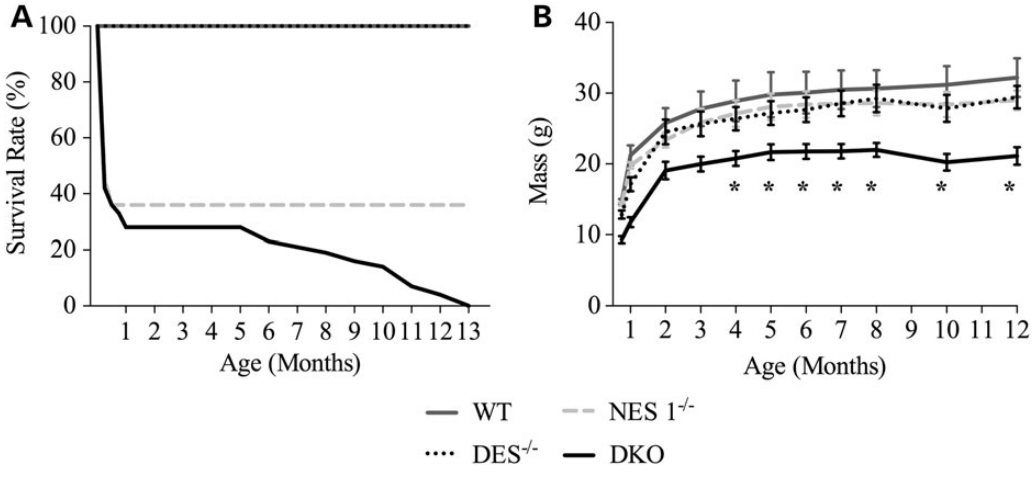

Figure 1. Disruption of both nesprin and desmin affects the life span and body weight of the mice. (**A**) Typical survival curve of wild-type (WT, $n = 90$), nesprin 1 (NES $1^{-/-}$, $n = 15$), desmin ($DES^{-/-}$, $n = 10$) and DKO ($n = 15$) mice. (**B**) Growth curve of aging mice, WT ($N = 12$), NES $1^{-/-}$ ($n = 12$), $DES^{-/-}$ ($n = 12$) and DKO ($n = 10$). Note that wild-type and $DES^{-/-}$ curves exactly overlap.

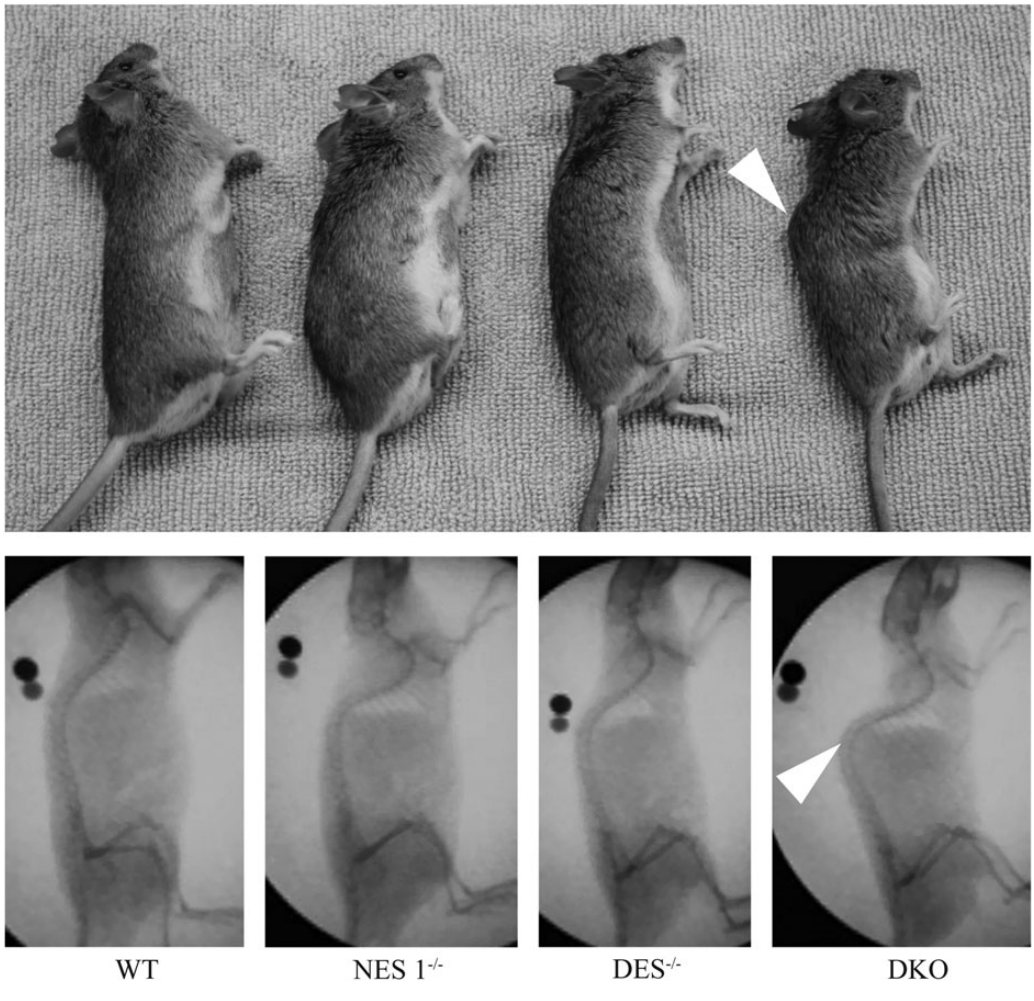

Figure 2. Kyphosis in DKO mice. Upper panel shows representative images of each genotype, with the white arrow indicating spinal kyphosis. Lower panel shows X-rays of the corresponding mice in the upper panel.

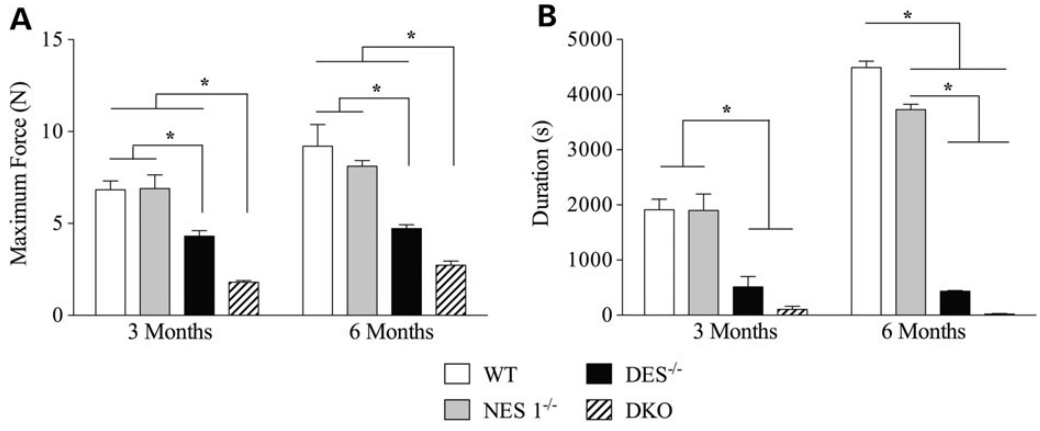

Figure 3. Strength and coordination are decreased in DKO mice. (**A**) Maximal force as measured by forelimb grip strength was significantly decreased in desmin and DKO animals at both 3 and 6 months of age compared with wild-type and nesprin $1^{-/-}$ animals ($P < 0.05$, via one-way ANOVA). Maximum force production of DKO animals was the lowest of all four groups at both 3 and 6 months of age. (**B**) The amount of time mice from each genotype were able to stay on a rotarod was recorded. At 3 months of age, wild-type and nesprin $1^{-/-}$ animals had a significantly longer duration time than both desmin and DKO animals. This was also true at 6 months of age, but the duration time for nesprin $1^{-/-}$ animals was also significantly shorter than wild-type mice (*$P < 0.05$, via one-way ANOVA) [$n = 5$ (WT), 6 (NES $1^{-/-}$), 7 (DES$^{-/-}$) and 8 (DKO)].

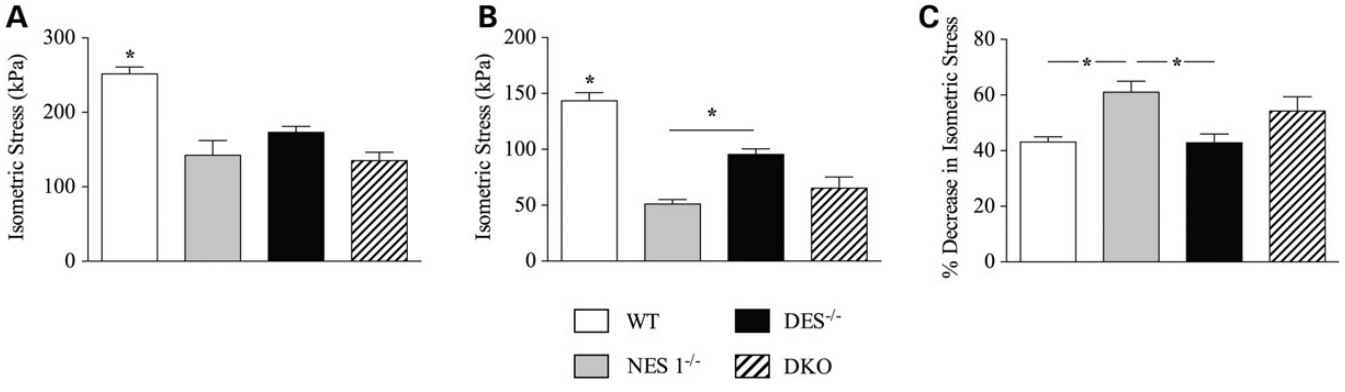

Figure 4. Stress production in DKO animals was identical to single-knockout mice. (**A**) Isometric stress production in wild-type animals was significantly higher than desmin$^{-/-}$, nesprin $1^{-/-}$ and DKO mice [$n = 10$ (WT), 8 (NES $1^{-/-}$), 8 (DES$^{-/-}$) and 11 (DKO)] (**B**) Following an injury protocol, stress production was decreased in all groups. It was found that the isometric stress for wild type was still significantly higher than the stress for the other three genotypes. Additionally, it was found that stress production in desmin$^{-/-}$ animals was significantly higher compared with nesprin 1 knockouts. (**C**) Percentage decreases in isometric stress following injury revealed that nesprin 1 null animals were the most susceptible to damage. The other three genotypes were statistically indistinguishable (*$P < 0.05$, via one-way ANOVA).

mice had the same duration, which was significantly higher than desmin$^{-/-}$ or DKO mice (Fig. 3B). By 6 months of age, wild-type animals had the longest duration and were able to stay on the rotarod for a significantly longer period of time compared with the other three genotypes (Fig. 3B). Desmin$^{-/-}$ and DKO animals had the shortest duration and were not significantly different from one another (Fig. 3B).

Stress production in DKO mice is affected to the same degree as single-knockout mice

Given the low force generation observed in DKO mice, we measured stress production to understand how muscle force was affected independent of cross-sectional area in DKO mice. Here, we measured stress production in the fifth toe of the extensor digitorum longus (EDL) muscle. When force was normalized to physiological cross-sectional area (PCSA), stress production in wild-type muscle was significantly higher compared with the other three genotypes (Fig. 4A). No differences were found among nesprin $1^{-/-}$, desmin$^{-/-}$ and DKO animals. These data suggest that DKO animals have no additional functional loss over single knockouts for either gene in terms of stress production. Muscle response to injury was also investigated by measuring stress production in the same muscles after 10 eccentric contractions (ECs). After muscle injury, wild-type stress production was still significantly higher compared with the other three genotypes; however, desmin$^{-/-}$ were not as affected by the injury compared with nesprin $1^{-/-}$ mice (Fig. 4B). Additionally, when examining percent decrease in isometric stress production, nesprin $1^{-/-}$ mice were significantly more injured compared with either wild-type or desmin$^{-/-}$ mice (Fig. 4C).

Tangent stiffness of skeletal muscle bundles and skeletal muscle fibrosis were increased in DKO mice

Passive mechanical properties are altered in desmin-null skeletal muscle owing to fibrosis (12). Therefore, in the present study, we determined how knockout of both desmin and nesprin 1 alters

muscle passive mechanics by mechanical testing of both single muscle fibers and fiber bundles. Single fiber testing, which is indicative of mechanical changes within muscle cells, revealed no genotypic differences (Fig. 5A). However, bundle testing, which reflects changes in the ECM, revealed a dramatic increase in tangent stiffness in DKO animals (Fig. 5B). These data demonstrate that there is a dramatic change in the ECM in the DKO model. Increased stiffness could stem from deposition of additional ECM, reorganization or crosslinking of the existing matrix proteins or a combination of the two. Thus, collagen content, the main component of the ECM, was quantified.

Collagen content of tibialis anterior (TA) muscles was determined using a modified hydroxyproline assay (26), as described in Materials and methods. Collagen content was lowest in wild-type and nesprin $1^{-/-}$ animals, with desmin-knockout samples being significantly more collagenous than wild type. Interestingly, DKO mice were significantly higher compared with both wild-type and nesprin $1^{-/-}$ muscles (Fig. 6A). ECM area fraction was then determined by examining laminin-stained cross-sections of muscle (Fig. 6B–F) as previously described (12). Similar to the collagen data, desmin$^{-/-}$ and DKO skeletal muscle had a higher ECM area fraction compared with wild type. Additionally, both the desmin$^{-/-}$ and DKO animals had a higher ECM area fraction compared with nesprin $1^{-/-}$ mice. Together these data demonstrate increased fibrosis in our DKO mouse model as well as desmin$^{-/-}$ animals.

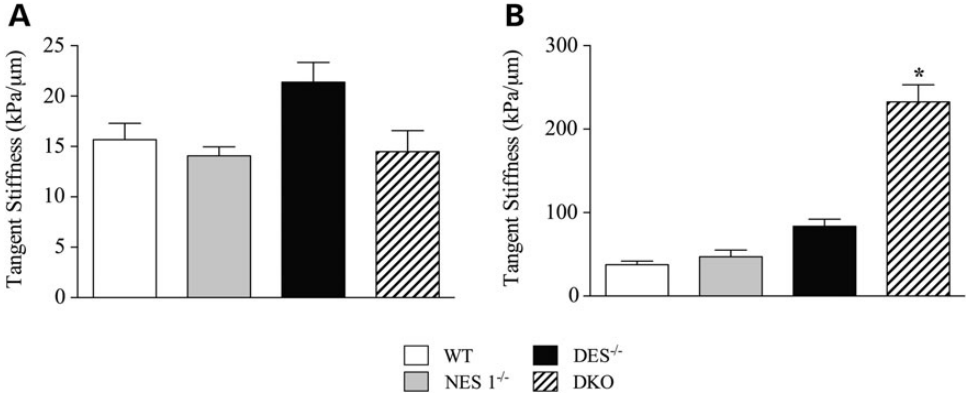

Figure 5. Passive mechanical testing showed increases in bundle stiffness, but not fiber stiffness, in DKO muscle. (**A**) Tangent stiffness values for each genotype from passive mechanical tests of single muscle fibers. No significant differences were found from the one-way ANOVA [$n = 11$ (WT), 8 (NES $1^{-/-}$), 10 (DES$^{-/-}$) and 13 (DKO)]. (**B**) Tangent stiffness values for each genotype from passive mechanical tests of muscle bundles. The tangent stiffness for the DKO was found to be significantly greater than the other genotypes ($^*P < 0.05$, via one-way ANOVA).

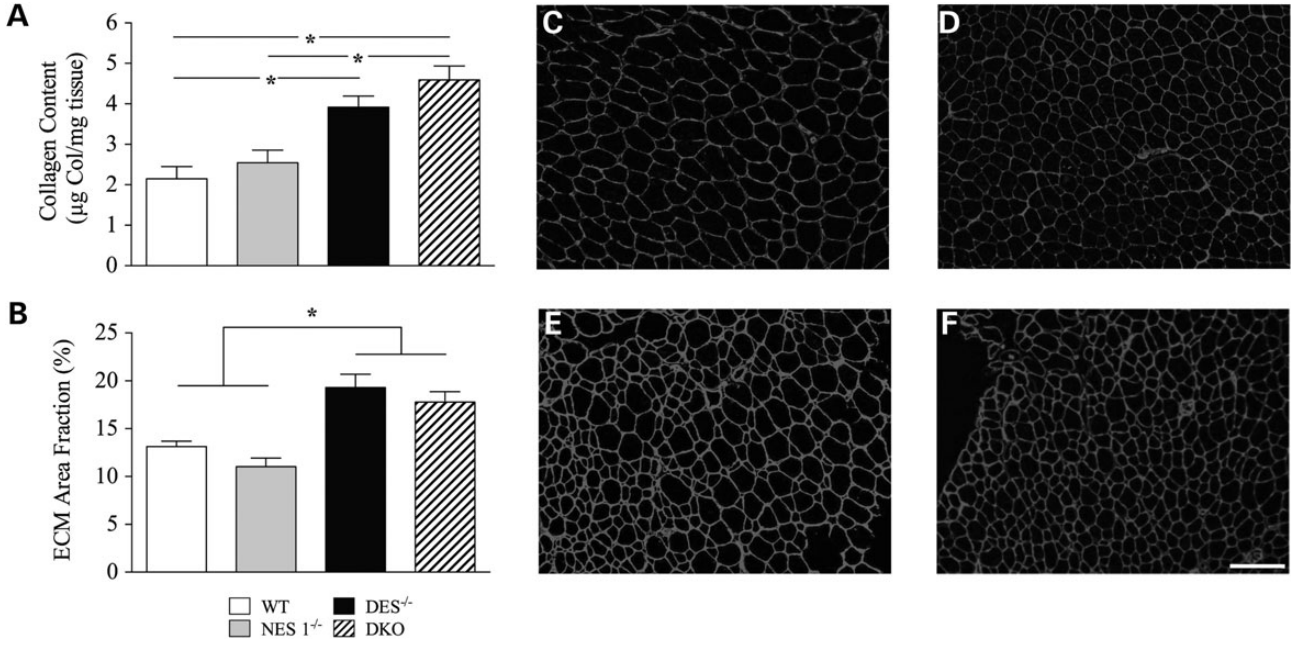

Figure 6. Skeletal muscle fibrosis occurs in desmin$^{-/-}$ and DKO mice. (**A**) Double-knockout samples were significantly more collagenous compared with the wild-type and nesprin 1 knockout samples, whereas the desmin-knockout samples were significantly greater than the wild-type samples ($^*P < 0.05$ one-way ANOVA) [$n = 8$ (WT), 7 (NES $1^{-/-}$), 7 (DES$^{-/-}$) and 13 (DKO)]. (**B**) ECM area fraction was also found to be elevated in both desmin and DKO muscle compared with wild type [$n = 10$ (WT), 6 (NES $1^{-/-}$), 10 (DES$^{-/-}$) and 13 (DKO)] (**C–F**). Laminin-stained samples of C—WT, D—NES $1^{-/-}$, E—DES$^{-/-}$, F—DKO. Scale bar = 100 μm.

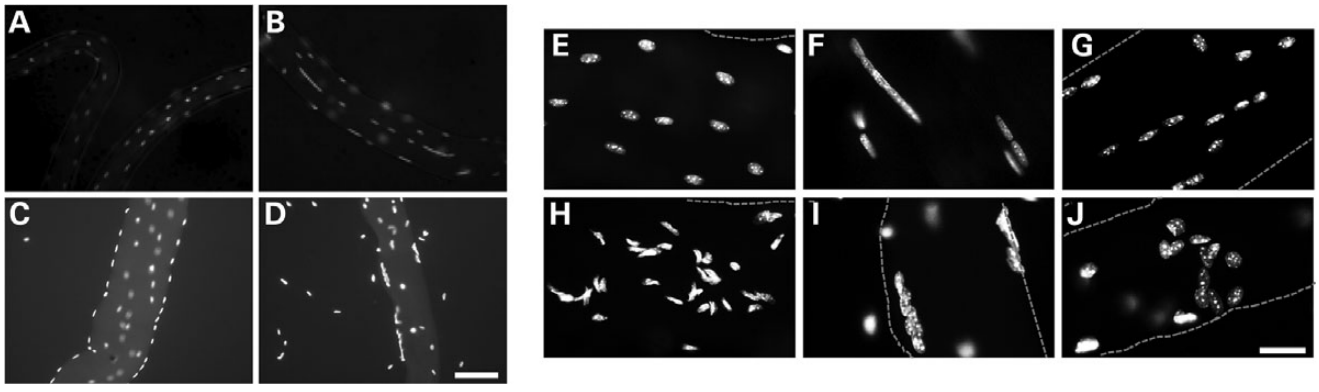

Figure 7. Nuclear anchorage defects. (**A–D**) Longitudinal images of single muscle fibers from 4-month-old mice using a 10× objective (A—WT, B—NES $1^{-/-}$, C—DES$^{-/-}$, D—DKO). Fibers were isolated from PFA-fixed soleus muscle and stained with DAPI. Note aggregation of nuclei in nesprin 1 and DKO fibers (B and D, respectively) compared with the evenly spaced nuclei in wild-type and desmin-knockout fibers (A and C, respectively). Additionally, some nuclei in DKO fibers have fallen away from the fiber. This is not seen in the other genotypes. Scale bar = 100μm. (**E–J**) Longitudinal images of single muscle fibers from 4-month-old mice under a 40× objective (E—WT, F—NES $1^{-/-}$, G—DES$^{-/-}$, H–J—DKO). Nuclei of wild-type (E) and desmin-knockout (G) mice were spherical in shape and were spaced evenly along the fiber. Nuclei in nesprin $1^{-/-}$ animals were clustered in lines within the muscle fiber (F). In DKO mice, the nuclei showed multiple shapes and were clustered together (H–J). Scale bar = 20 μm.

Nuclear anchorage and localization defect in skeletal muscles of mice with dual nesprin and desmin ablation

Given that both nesprin 1 and desmin interact with nuclei in skeletal muscle, we further interrogated our mouse models to examine potential alterations in nuclear anchorage. Nuclear shape and localization patterns were examined by fluorescence imaging of DAPI-stained single fibers from soleus muscle. In wild-type fibers, nuclei were spaced evenly along the fiber length (Fig. 7A). Desmin$^{-/-}$ nuclei had a similar pattern to wild-type mice (Fig. 7C). As previously described (5), nuclei of nesprin $1^{-/-}$ mice were distributed along the length of the muscle fiber but were in lines and clusters not observed in wild-type or desmin$^{-/-}$ animals (Fig. 7B). Interestingly, nuclei of DKO mice were significantly clustered, and some were detached from the fiber (Fig. 7D).

Under a 40× objective, wild-type and desmin$^{-/-}$ nuclei were spherical in shape and evenly spaced along the fiber (Fig. 7E and G). Nesprin $1^{-/-}$ nuclei were aggregated together in lines along the length of the muscle fiber (Fig. 7F). In DKO mice, the nuclear patterns seen were qualitatively different from the other three genotypes (Fig. 7H–J). Here, significant irregular nuclear clusters were observed in various locations along the length of the fiber (Fig. 7I and J). Additionally, in many locations, it was observed that a number of nuclei had detached from the fiber, indicating compromised nuclear anchorage in DKO mice (Fig. 7I). Finally, irregular individual nuclear shapes were observed in numerous imaging fields of DKO muscle fibers (Fig. 7H–J). These data suggest that nuclear anchorage is aberrant in DKO mice compared with controls.

To further quantify nuclear patterns, mice with GFP-labeled nuclei were generated by crossing mice with a nuclear-restricted GFP (H2B-GFP) cassette driven by the obscurin promoter (27) with nesprin 1 and desmin mutant mice. Creation of these mice allowed us to examine skeletal muscle nuclei without staining nuclei of other cell types. Moreover, this model permitted imaging of entire muscle bundles under confocal microscopy and examination of three-dimensional spatial changes in response to loss of nesprin 1 and/or desmin (Fig. 8; Supplementary Material, videos S1–S8). As previously shown, wild-type and desmin$^{-/-}$ animals displayed a uniform distribution of nuclei along the length of the muscle fiber with a similar distribution of nuclear volumes in both the soleus and TA muscles (Fig. 8A and B, Supplementary Material, videos S1–S8). Nuclear aggregation was not observed in wild-type samples, and it was primarily absent in desmin$^{-/-}$ samples except for small areas observed in the soleus muscle (Fig. 8A and B). Nuclei of nesprin $1^{-/-}$ were again visualized as aggregates, where the soleus and TA muscles showed increased nuclear cluster volume as determined using Volocity Software (PerkinElmer, Waltham, MA, USA) (Fig. 8A and B). As was seen in DAPI-stained single fibers, 3D reconstructions of DKO nuclei in muscle bundles revealed a dramatic alteration in nuclear anchorage (Fig. 8A and B, Supplementary Material, videos S1–S8). Large aggregates composed of several nuclei were seen in soleus and TA muscles of DKO animals in a manner not seen in the other three genotypes. Soleus and TA nuclear cluster volume distributions were dramatically shifted toward larger values in DKO mice (Fig. 8A and B). This shift in nuclear cluster volume indicates an increase in both the size and abundance of nuclear clustering in DKO mice over WT and single-knockout animals.

Mice with ablation of nesprin and desmin present with decreased nuclear deformation under biomechanical stretch

Investigation of nuclear morphology and localization in the above images only provides information on nuclear placement within the muscle fiber. It is unclear how strain transmission between the nucleus and cytoskeleton is affected in DKO animals. To examine strain transmission, single nuclei were imaged during controlled deformation of muscle bundles. When TA muscle bundles were stretched, nuclei of each genotype were deformed to different extents (Fig. 9A). The amount of nuclear deformation was indicated by quantifying the nuclear aspect ratio of each nucleus at increasing sarcomere lengths (Fig. 9B). The slope of aspect ratio versus sarcomere length line indicated the amount of deformation imposed upon the nucleus by the cytoskeletal network (Fig. 9C). Nuclei from all four genotypes deformed linearly; however, the extent of

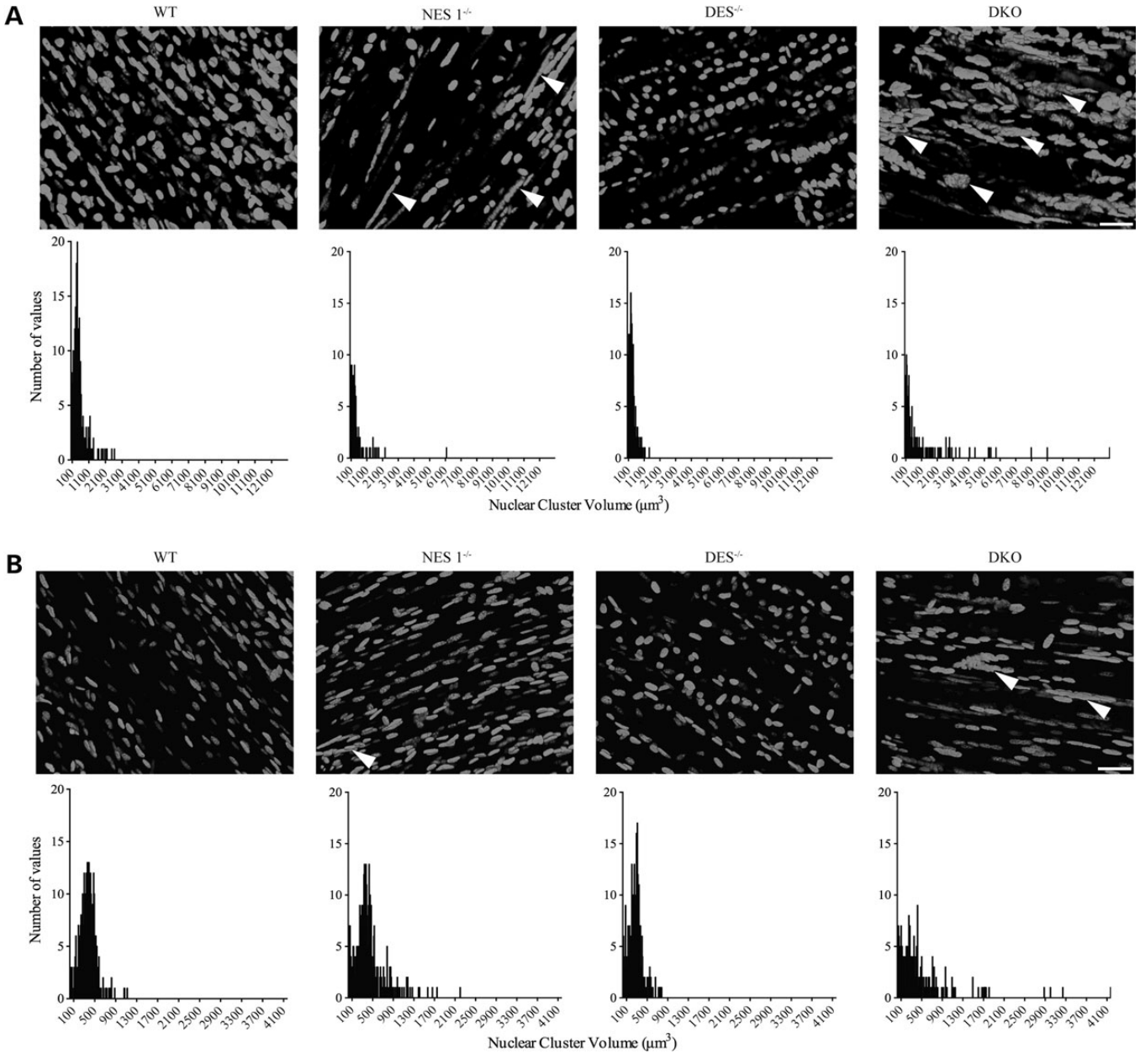

Figure 8. Elevated levels of nuclear clustering were observed in DKO mice. Dissected muscles were fixed by PFA overnight, and then, bundles were dissected out of the muscle. The small bundles were mounted onto slides and imaged using a confocal microscope. The images were collected and analyzed by Volocity software. (**A**) Nuclei of soleus muscle bundles from 4-month-old mice. In DKO animals, the nuclei were clustered together in large aggregates that are not seen in the other genotypes. Nuclei of nesprin-null animals were slightly clustered in lines throughout the muscle bundle. Nuclei of WT and DES$^{-/-}$ bundles were spaced evenly. Nuclear cluster volume distributions in the lower panel of (A) demonstrate increased cluster volumes in both nesprin-null and DKO soleus muscle. (**B**) Nuclei of TA muscle bundles from 4-month-old mice. In both nesprin-null and DKO animals, nuclear clustering is increased as observed visually and graphically. White arrows indicate nuclear clusters. Scale bar = 20 μm in all images.

deformation was altered in nesprin 1$^{-/-}$ and DKO animals. Nuclei of nesprin 1$^{-/-}$ and DKO mice deformed significantly less compared with wild-type and desmin$^{-/-}$ nuclei ($P < 0.05$).

Ultrastructural and immunofluorescent examination of myonuclei from mice with ablation of nesprin and desmin reveal nuclear aggregation and altered chromatin compaction

Transmission electron microscopy was used to examine the nuclear phenotype of DKO muscles. In wild-type and desmin$^{-/-}$ soleus muscle, single nuclei were observed along the periphery of the muscle fiber with no clustering observed (Fig. 10A and C). As seen with light microscopy, TEM showed nesprin 1$^{-/-}$ nuclei clustered in lines along the muscle fiber periphery (Fig. 10B). TEM micrographs also revealed that DKO mice had severe aggregation of nuclei in muscle tissue compared with WT and single-knockout mice (Fig. 10D). Qualitative observations of these images revealed changes in electron dense regions at the nuclear envelope (Fig. 10D, yellow arrows). These indicate a change in chromatin compaction and

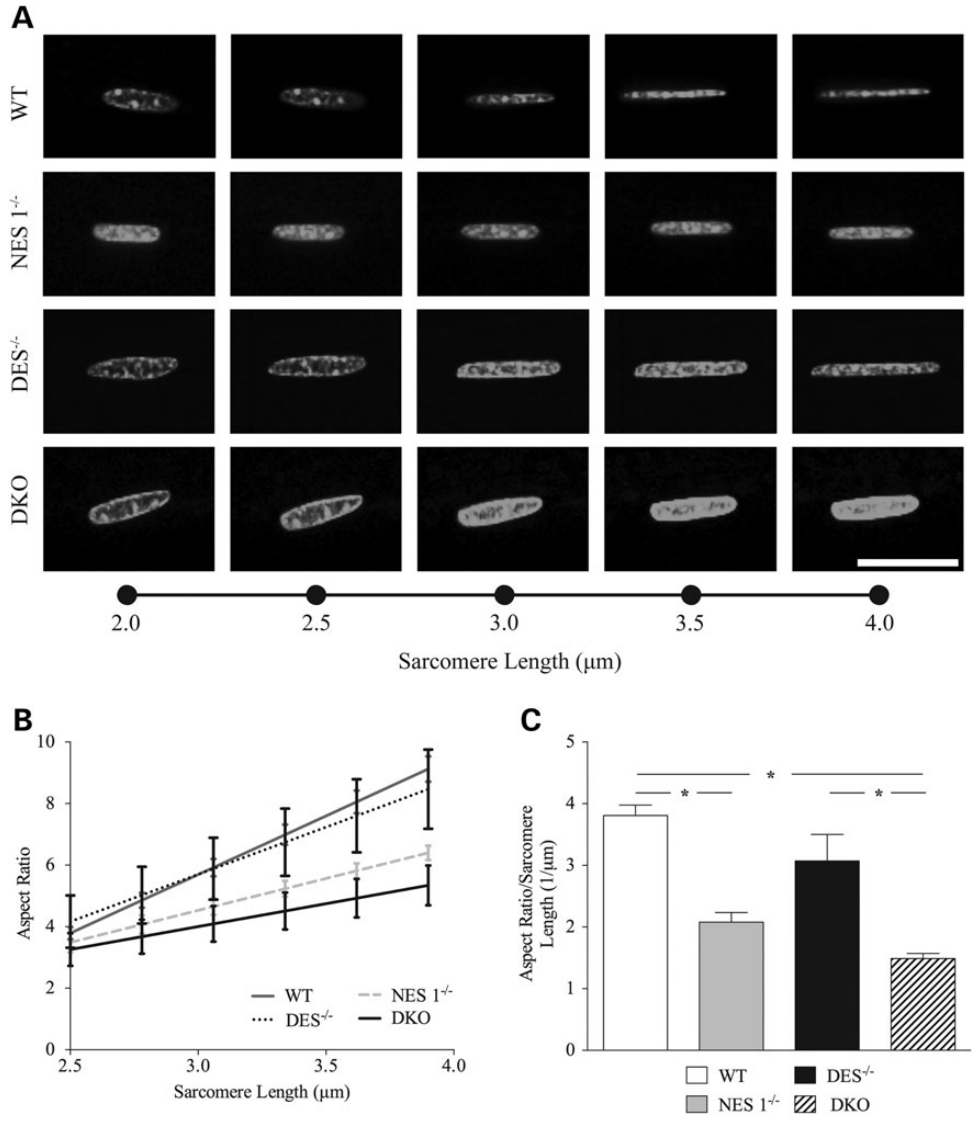

Figure 9. Cytoskeletal-nuclear strain transmission is dramatically reduced in DKO skeletal muscle. (**A**) Nuclear deformation caused by a controlled deformation of muscle bundles in the TA muscle. Wild-type and desmin-knockout nuclei deformed, whereas this deformation was attenuated in the nesprin 1 and DKO mice. Scale bar = 25 μm (**B**) Nuclear aspect ratio versus sarcomere length. The trend line is an average of the trend lines from each experiment. (**C**) Slope of the aspect ratio versus sarcomere length for each genotype. A larger slope correlates to more deformation. The nuclear deformation in the wild-type and desmin-knockout mice was significantly greater than that observed in the nesprin 1 and DKO mice. $n = 3$ mice/group ($^*P < 0.05$, via one-way ANOVA).

loss of heterochromatin, similar to other models of nuclear anchorage loss (6).

To quantify this change in chromatin compaction, we examined localization of chromatin and heterochromatin protein 1 beta (HP1β) (28,29). HP1β interacts with methylated histone H3 and plays a key role in heterochromatin maintenance (30,31). A reduction in co-localization of DRAQ5, a fluorescent DNA stain and HP1β would suggest altered chromatin compaction/localization to confirm observed loss of compacted chromatin by TEM (Fig. 10D) (32). Dual ablation of both nesprin and desmin resulted in a reduced interaction of DRAQ5 and HP1β as visualized by immunofluorescence and quantitative Pearson's correlation coefficients (Fig. 10E and F). These data indicate that loss of nuclear anchorage results in altered patterns of chromatin compaction/localization. Taken together, we conclude that loss of both nesprin 1 and desmin causes an aggregation of nuclei and alerted chromatin compaction.

DISCUSSION

A key feature of skeletal muscle that affects its development and phenotype is the linkage of the nucleus to the cytoskeleton (3–5). A number of skeletal muscle pathologies, including EDMD, have been directly linked to proteins associated with myonuclei. Thus, understanding the factors involved in nuclear anchoring and positioning can reveal the importance of nuclear connectivity in skeletal muscle. Therefore, in this study, we examined two proteins that are involved in nuclear anchorage, nesprin 1 and desmin. Herein, we demonstrate that dual ablation of nesprin 1 and desmin results in increased muscle weakness, loss of

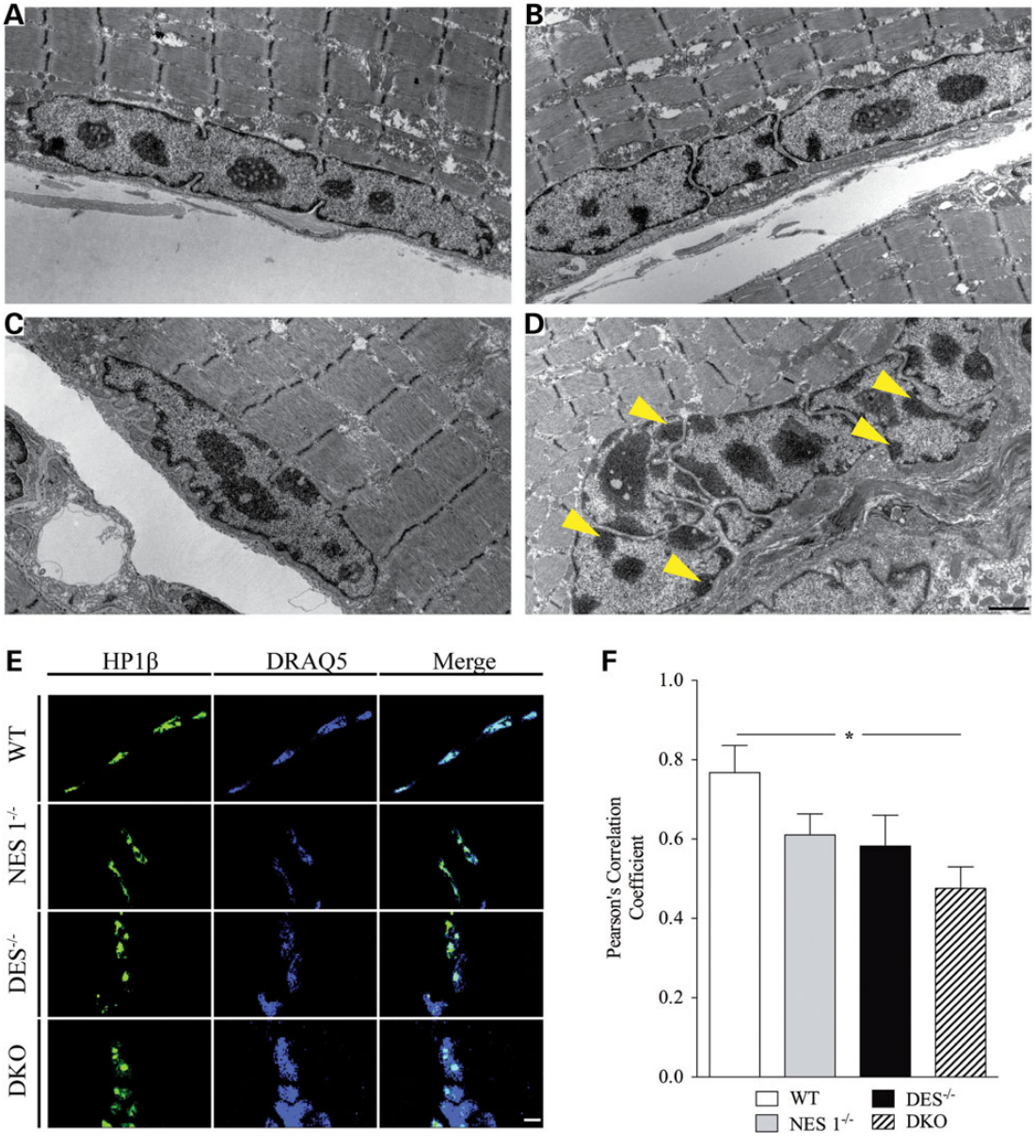

Figure 10. Ultrastructural and chromatin localization analyses of skeletal muscle. **(A–D)** Nuclei of wild-type (A) and desmin-null (C) skeletal muscle were properly localized at the periphery of the cell, and no clustering was observed. TEM showed nuclear clusters in nesprin $1^{-/-}$ skeletal muscle (B). DKO micrographs of myonuclei showed severe nuclear aggregation and heterochromatin morphology changes (yellow arrows) (D). **(E)** Representative images of heterochromatin 1 beta (HP1β) (green) and DRAQ-5 (blue) staining in adult skeletal muscle. **(F)** Quantitative co-localization examination of HP1β and DRAQ5 via Pearson's Correlation Coefficient image analyses. Co-localization of HP1β and DRAQ-5 was significantly decreased in DKO muscle, indicating a disruption in the heterochromatin structure. TEM—scale bar = 1 μm, Fluorescence—scale bar = 5 μm. (*$P < 0.05$, via one-way ANOVA).

nuclear anchorage and positioning, defective chromatin localization, decreased nuclear-cytoskeletal strain transmission and increased skeletal muscle fibrosis compared with the three other models examined.

Prior observations demonstrated that knockout of either nesprin 1 or desmin resulted in skeletal muscle defects as well as partial loss of nuclear anchorage and nuclear deformation under tensile loading (5,7). A nesprin 1 global ablation model resulted in partial nuclear anchorage and nuclear-cytoskeletal strain transmission defects (5). Loss of desmin alone was also shown to result in mild nuclear anchorage defects as well as a progressive skeletal muscle fibrosis phenotype (7,12).

In a previous study, our laboratory found that the mortality rate for nesprin 1 knockout animals was ~60% by 1 month of age (5). A similar mortality rate for those animals was seen in this study for nesprin 1 knockout mice; however, ablation of both nesprin 1 and desmin resulted in increased mortality rates (Fig. 1A). We found that at 13 months of age, there were no surviving DKO mice. This is a striking finding compared with the nesprin 1 null animals, where 40% of animals remain alive at 13 months of age. This increased mortality rate in DKO animals can likely be attributed to the observed muscle wasting and weakness in these mice. In addition to the high mortality rate observed in DKO animals, there was an increase in severity of dystrophic

phenotypes, such as muscle weakness and fibrosis. Evidence of muscle wasting was present in DKO animals in the form of decreased body weight, increased incidence of kyphosis and decreased muscle strength (Figs 1B, 2 and 3A). These data demonstrate that severe defects in skeletal muscle result with the loss of both nesprin 1 and desmin. Interestingly, when active mechanical studies were performed that took muscle PCSA into consideration, muscle stresses in DKO animals were not significantly different from their single-knockout littermates (Fig. 4A). These data demonstrate that low force production in DKO mice is due to the smaller size of these mice and their smaller muscles and that DKO mice have no additional functional loss compared with single-knockout animals with regard to stress production.

Skeletal muscle fibrosis is a major clinical problem resulting in muscle weakness and a loss of flexibility (33). Previous studies showed that desmin deletion results in a progressive skeletal muscle fibrosis phenotype (12). Our data are consistent with this study showing elevated tangent muscle bundle stiffness and collagen content in desmin-null skeletal muscle. More striking was the observation that muscle tangent stiffness of DKO samples was six times greater compared with wild-type samples. This large increase in tissue stiffness demonstrates that a dramatic fibrotic response resulted from ablation of both nesprin 1 and desmin. In addition to an increase in tissue stiffness, collagen content was also increased in DKO skeletal muscle. Collagen content does not correlate with passive mechanical data (Figs 5 and 6). When plotted against each other, the tangent stiffness versus collagen content graph reveals no relationship (Supplementary Material, Fig. S1). This is especially evident when looking at the points within each genotype. The weak correlation suggests that there is another factor that explains the dramatic increase in mechanical stiffness with increased collagen. Since collagen did not become much more abundant in DKO muscle, a possible explanation is that collagen organization, not collagen quantity, was altered. Crosslinks within the collagen molecule, which have been implicated in both cardiovascular and pulmonary fibrosis, could also be causing this increase in the tangent stiffness (34,35). Additionally, collagen fibril orientation and organization may be responsible for this increased stiffness, but additional studies would have to be conducted to verify this.

One of the most dramatic results from this study was the effect that knocking out both nesprin 1 and desmin had on nuclear localization and anchorage (Figs 7–9). It is well established that myonuclei in healthy skeletal muscle are spaced evenly along the fiber length and maintain a particular myonuclear domain size (36). It has been hypothesized that in order to minimize transport from nuclei, each nucleus is ‘assigned’ to a particular region to fulfill the needs of the adjacent cytosolic volume (36). For the vast majority of cases, nuclei in skeletal muscle are spaced as far apart from each other to presumably minimize transport distances between the nucleus and cytosol (36). Loss of nuclear-cytoskeletal connections in the current study resulted in large clusters of nuclei throughout different muscles of DKO animals. The large clusters of nuclei in DKO animals could imply that transport distances are not minimized and certain domains within the muscle may not be receiving the necessary signals for proper function. A lack of proper nuclear localization and aberrant nuclear clumping could explain the more severe phenotype seen in these DKO animals. With transport distances not minimized between the cytosol and nuclei, certain factors, such as mRNA transcripts, may not be able to reach their targets. This may result in protein production remaining limited to small areas surrounding these nuclear clumps. Limited spatial distribution of proteins could potentially inhibit muscle size, causing the stunted skeletal muscle growth and weakness observed in DKO mice. This is a potential explanation of why we observe decreased muscle strength, but not decreased stress production in DKO mice over controls; however, future work is needed to address this question.

Similar to our previous study in nesprin knockout animals, we observed that nuclei of nesprin-null animals had decreased nuclear deformability compared with wild-type animals (5). Decreased nuclear deformation was also found in DKO animals (Fig. 9). Limited nuclear deformation suggested that mechanical integration between the nucleus and the cytoskeleton was reduced in nesprin $1^{-/-}$ and DKO mice. Although not significantly different from nesprin $1^{-/-}$, the DKO trended toward less nuclear deformation.

Collectively, we have shown that ablation of both nesprin 1 and desmin dramatically reduced connectivity of the nucleus to the cytoskeletal network in skeletal muscle. Globally, this lack of nuclear connectivity coincides with a decrease in muscle strength, drastically shorter lifespans and a decrease in adult mass. With regard to skeletal muscle specifically, it was found that myonuclei in DKO mice had a decrease in nuclear-cytoskeletal strain transmission. This loss of nuclear connectivity coincided with a fibrotic tissue response as marked by increases in tissue stiffness, collagen content and ECM area fraction. Together these results suggest that nesprin 1 and desmin play redundant roles in nuclear anchorage in skeletal muscle, and this loss of connectivity could potentially explain the observed pathology in our DKO mice. Future research into the connection between nuclear anchorage and our observed dystrophic phenotypes is necessary to elucidate a mechanism behind how these may be causally related. This future research could allow us to better understand and develop treatments for disorders associated with nuclear connectivity defects, muscle weakness and fibrosis, such as EDMD.

MATERIALS AND METHODS

Generation of nesprin and desmin DKO mice

Previously, we generated nesprin 1 knockout mouse (5), and desmin-knockout animals were generated elsewhere (22). To establish DKO lines, nesprin $1^{+/-}$ and desmin$^{+/-}$ were crossed to generate nesprin $1^{+/-}$; desmin$^{+/-}$ double heterozygous mice. Double heterozygous mice were crossed with each other to generate four groups: homozygous wild-type, nesprin 1 knockout (nesprin $1^{-/-}$), nesmin knockout (desmin$^{-/-}$) and DKO mice for experiments. All mice were maintained on a mixed Black Swiss and 129/SvJ background.

Mouse survival and growth curve determination

Murine survival was assessed as previously described (5). In this study, 90 wild-type, 15 nesprin $1^{-/-}$, 10 desmin$^{-/-}$ and 15 DKO animals were examined for up to 1 year of age. Time points were collected at t = birth, 1 week, 2 weeks, 3 weeks and at 1–13

months of age. Growth curves for each genotype were determined as previously described (5). Briefly, body weights were determined by weighing mice from each genotype [WT ($n = 12$), NES $1^{-/-}$ ($n = 12$), DES$^{-/-}$ ($n = 12$), DKO ($n = 10$)], at 3 weeks, 1–8 months, 10 months and 12 months of age.

Single fiber isolation and staining

Single myofibers were obtained from soleus and TA muscles fixed with 4% paraformaldehyde (PFA) overnight. Fixed muscles were divided into bundles by pulling the tendon with forceps and removing non-muscle tissue under a binocular microscope. Single muscle fibers were teased out of muscle bundles. Isolated myofibers were rinsed twice with phosphate-buffered saline (pH 7.2) for neutralization. Fibers were then mounted in mounting medium with DAPI (Vector, H1200).

Maximum force generation and rotarod duration time

Maximum force production was determined by having mice grab onto a bar with their forelimbs [$n = 5$ (WT), 6 (nesprin $1^{-/-}$), 7 (desmin$^{-/-}$), 8 (DKO)]. This bar was linked to a force transducer, and when the tail was pulled back by hand, maximum force was recorded. In order to assess coordination, balance and endurance, mice were placed onto a rotarod, and the amount of time they were able to stay on was recorded. The rotarod protocol was as follows: 0.1 m/min for 3 min, and then speed was increased by 0.02 m/min, up to 0.35 m/min. The rotarod duration time was recorded when the mice became exhausted and fell down.

Histology

The TA muscle isolated from 1-month-old mice were [$n = 10$ (WT), 6 (NES $1^{-/-}$), 10 (DES$^{-/-}$), 13 (DKO)] pinned under tension, flash-frozen in liquid nitrogen-cooled isopentane and stored at -80°C until further processing. A section from the midline ($\sim$1 mm) of the TA was cut out of the muscle with a razorblade. The section was carefully placed in OCT with muscle fibers oriented such that transverse sections would be cut from the muscle. Sections of 10 μm were cut from OCT-embedded samples on a cryostat at -20°C (Microm HM500, Waldorf, Germany) and stained for laminin to visualize the extracellular space. Samples were blocked with BSA and incubated overnight with a primary antibody to laminin (rabbit polyclonal, Sigma, St. Louis, MO, USA). Samples were then treated with an Alexa-Fluor 594 goat anti-rabbit immunoglobin G (Invitrogen) secondary antibody. ECM area fraction was determined from laminin-stained cross-sections as previously described (12). Image background was subtracted such that fiber centers were set to a value of 0 in the RGB channel. A threshold was then applied to the images in which the amount of white (stained) pixels was determined as a percentage of total area. Image processing parameters were standardized between images to ensure no bias. Each image was inspected for blood vessels and areas of poor staining prior to analysis, and those regions were removed from the quantification.

Immunofluorescent staining and analyses

Three-month-old mouse soleus muscles from WT, nesprin $1^{-/-}$, desmin$^{-/-}$ and DKO mice (three biological replicates per condition) were stained as previously described (6) for HP1β (Cell Signaling Technology, Danvers, MA, USA). Nuclei were also stained using DRAQ5 (Cell Signaling Technology), a fluorescent DNA stain that binds to the A–T minor groove. Samples were imaged using a 60× objective with glycerol immersion using an inverted confocal microscope (Confocal microscope used was actually Leica SP5). Approximately 200+ nuclei were imaged per condition and used for Pearson's Correlation Coefficient analyses, performed via Volocity high performance 3D imaging software (PerkinElmer).

Active mechanics

Active mechanical testing was performed on the fifth toe belly of the EDL muscle on 1-month-old mice [$n = 10$ (WT), 8 (nesprin $1^{-/-}$), 8 (desmin$^{-/-}$), 11 (DKO)] as previously described (37). Dissection was performed in mammalian Ringer's solution containing (in mM): NaCl (137), KCl (5), NaH_2PO_4 (1), $NaHCO_3$ (24), $CaCl_2$ (2), $MgSO_4$ (1) and glucose (11) containing 10 mg/l curare. Following removal of the TA, the EDL was made visible. The second, third and fourth toe bellies of the EDL were carefully dissected away one-by-one using a 30-gauge needle to cut away connective tissue. Once the superfluous muscle bellies were cut away, only the fifth toe of the EDL remained. 6–0 silk sutures (Teleflex Medical, Coventry, CT) were tied around the proximal and distal tendon of the muscle as close to the fibers as possible to minimize tendon-series compliance. The proximal and distal tendons were then transected, releasing the fifth toe of the EDL. The muscle was placed into a custom chamber with Ringer's solution, the distal tendon was secured to the arm of a dual-mode ergometer (model 300B; Aurora Scientific, Richmond Hill, ON, Canada), and the proximal tendon was secured to a fixed medal pin. Muscle slack was taken up, and muscle length was measured. The muscle was then stretched by 15%, which typically corresponded to a sarcomere length of 3.0 μm. The sarcomere length was confirmed by laser diffraction, and if the sarcomere length was not 3 μm, it was adjusted accordingly. The fiber length was measured. To determine the voltage that would yield maximal force production, the muscle was stimulated with an electrical stimulator (model S88; Astro-Med, West Warwick, RI, USA) via platinum plate electrodes that extended the length of the EDL. Muscle twitches were administered beginning with a twitch voltage of 4 V. The twitch voltage was increased by 1 V until the output by the muscle no longer increased with an increase in twitch voltage. This peak twitch voltage was doubled, and then a bout of three isometric contractions (400-ms train of 0.3-ms pulses at 100 Hz) was administered at this voltage with 2-min of rest between each fused tetanus. Following this bout of contractions, the muscle was subjected to a bout of 10 ECs. The EC begins with maximally stimulating the muscle, and 200 ms into the contraction, the muscle was forcibly lengthened by 15% fiber length at 2 fiber lengths/s. Then, the stimulus ended, and the muscle returned to its starting length. This process was repeated for a total of 10 times with 3-min rest between contractions. Three isometric contractions were then imposed on the muscle to determine how much the muscle had been damaged. Following the final isometric contraction, the muscle was removed from the chamber, blotted dry and weighed. The maximum force values were converted

into maximal stress values by dividing by the PCSA.

$$\text{PCSA} = \frac{\text{mass} \times \cos(\theta)}{\rho \times F_l},$$

where θ represents pennation angle; ρ, muscle density (1.056 g/cm^3); and F_l, fiber length.

Passive mechanics

Passive mechanical testing was performed on single fibers and bundles from the TA muscle [$n = 11$ (WT), 8 (nesprin $1^{-/-}$), 10 (desmin$^{-/-}$), 13 (DKO)] as previously described (38). These samples were collected from the contralateral side of the same 1-month-old mice used for the histological analysis. TA samples were isolated from the lower limb and stored in a storage solution at −20°C for up to 2 weeks containing (in mM): K-propionate (170), K_3EGTA (5), $MgCl_2$ (5.3), imidazole (10), Na_2ATP (21.2), NaN_3 (1), glutathione (2.5), leupeptin (0.05) and 50% (vol/vol) glycerol. Before passive mechanical testing, samples were transferred to a relaxing solution as described earlier. Single muscle fibers as well as bundles of fibers were dissected out of the TA and secured in a custom chamber. On one side, the sample was secured to a force transducer (Aurora Scientific 405A; Aurora, ON, Canada) and the other side was secured to a titanium wire rigidly attached to a rotational bearing (Newport MT-RS; Irvine, CA, USA). Once securely attached, the sample was elongated to take up the slack and register a force just above the noise level (∼1 mN for fibers and ∼20 mN for bundles). Slack sample length (L_0) was measured as the loop–loop distance, and the diameter was measured in three different locations along the sample. Sarcomere length was measured by laser diffraction using a low-powered laser diode. An incremental stress-strain protocol was then implemented on the sample. Samples were stretched by 10% L_0 at a strain rate of 20 FL/s and then allowed to stress-relax for 3 min. Fibers were stretched until failure, or achieving a sarcomere length of 4 μm, whichever occurred first. At the end of each stress-relaxation period, the force and sarcomere length were recorded. Stress was calculated by dividing the recorded force by the cross-sectional area of the sample. Sample cross-sectional area was calculated from the initial sample diameter, assuming that the sample was an isovolumic cylinder (39). The tangent stiffness was calculated by fitting a quadratic equation to the stress–sarcomere curve and calculating the slope at a sarcomere length of 3.2 μm.

Hydroxyproline assay

Collagen content of TA muscles was determined using a modified version of a previously published protocol (26). The collagen content of TA samples from 1-month-old mice, previously used for histological analysis, was quantified [$n = 8$ (WT), 7 (nesprin $1^{-/-}$), 7 (desmin$^{-/-}$), 13 (DKO)]. Six to ten thick (35 μm) sections were cut from OCT-embedded samples using a cryostat at −20°C (Microm HM500). The OCT was carefully peeled away from each section, leaving only muscle tissue. These sections were placed into the pre-weighed Eppendorf tubes, and the tubes were weighed again to determine the mass of each sample. 6 M HCl was pipetted into each tube at a concentration of 5 mg of sample per milliliter of acid. Samples were placed in an oven at 110°C for 24 h for digestion. Following sample digestion, standards of hydroxyproline (OHP) were made at varying concentrations. OHP standards and samples were pipetted, in triplicate, onto a 96-well plate. The 96-well plate was then placed into a vacuum desiccator where the standards and samples were evaporated to dryness (∼1 h). Once the samples in the 96-well plate were dried, a chloramine-T solution was added to each well, and the samples were incubated for 20 min at room temperature with gentle agitation. The standards and samples were then incubated with a para-dimethylaminobenzaldehyde solution for 30 min at 60°C. Absorbance readings at 550 nm were taken using a spectrophotometer, and the amount of collagen in each sample was calculated by using a hydroxyproline to collagen conversion factor of 7.46.

Transmission electron microscopy

For TEM analysis, samples were prepared as previously described (40). Mice were first anesthetized with Ketamine with Xylene and subsequently perfused through the left ventricle with Tyrode's buffer including 50 mM KCl, followed by fixative (2% paraformaldehyde, 2% glutaraldehyde in PBS, pH 7.4). The muscles examined were removed, diced and kept in fixative overnight. Samples were then washed three times with 0.15 M sodium cacodylate buffer and then post-fixed with 2% OsO4 in 0.15 M sodium cacodylate buffer for 1 h. The following day, tissues were stained overnight in 2% uranyl acetate, dehydrated and embedded into Durcupan resin (EMD, Gibbstown, NJ, USA) using a standard method. Ultra-thin sections (60–70 nm) were stained with 2% uranyl acetate and statured lead citrate solution and observed with a JEOL-1200EX transmission electron microscope at an accelerating voltage of 80 kV.

Examination of skeletal muscle nuclear positioning

To examine nuclear positioning, we first generated obscurin H2BGFP+ mice as previously described (27). Briefly, expression of nuclear-tagged GFP was driven by the obscurin promoter, which is limited to cardiac and skeletal muscle, thus allowing for examination of nuclei labeled only in these tissues. We then generated and crossed these mice to our nesprin $1^{-/-}$; obscurinH2BGFP+, desmin$^{-/-}$; obscurinH2BGFP+ and nesprin $1^{-/-}$:desmin$^{-/-}$; obscurinH2BGFP+ lines. Three-dimensional analysis was performed as previously described (6,41).

Nuclear deformation

Nuclear deformation testing was performed on muscle bundles from TA muscles of 3-month-old mice as previously described (42). Samples were isolated from three animals per group (WT, nesprin $1^{-/-}$, desmin$^{-/-}$ and DKO) with four bundles per animal and approximately four nuclei per bundle tested. Tibialis anterior muscles were isolated and separated from the lower limbs and placed into a relaxing solution at pCa 8.0 and pH 7.1 containing (in mM): imidazole (59.4), KCH_4O_3S (86), $Ca(MSA)_2$ (0.13), $Mg(MSA)_2$ (10.8), K_3EGTA (5.5), KH_2PO_4 (1), leupeptin (0.05) and Na_2ATP (5.1) for 30 min. Muscle bundles were carefully dissected out and secured into a custom

apparatus with 10–0 monofilament nylon suture. The apparatus was made by a modifying a Lab-Tek^{TM}4-chambered cover glass (Thermo Fisher Scientific; Waltham, MA, USA) depicted in Figure 1. The cover glass was modified by securing a dissecting pin in paraffin wax on one side of the chamber, and another dissecting pin, held in place with SYLGARD® (Dow Corning; Midland, MI), was threaded through a hole drilled into the side of the chamber on the other side of the cover glass. A hypodermic needle was crimped onto this pin, which allowed for stretching of the secured muscle bundles. Bundle length was measured, and the chamber was secured onto a custom made stage of an inverted confocal microscope (Confocal microscope used was actually Leica SP5). Bundles were stretched using a micrometer until all slack was taken up. Four nuclei were imaged at slack length, slack sarcomere length was determined from the bright field image, and then the bundles were stretched in sarcomere length increments of $\sim$0.25 μm until achieving a sarcomere length of $>$4.0 μm. After each stretch, the same nuclei were imaged and the sarcomere length was recorded. Changes in nuclear aspect ratio with increasing strain were determined using ImageJ (NIH, Bethesda, MD, USA).

SUPPLEMENTARY MATERIAL

Supplementary Material is available at *HMG* online.

ACKNOWLEDGEMENTS

The authors thank Shannon Bremner and Blair Conner for their technical assistance.

Conflict of Interest statement. None declared.

FUNDING

This work was supported by grants from the National Institute of Health (AR059334 and HL106968 to J.C.; AR061303, HD050837 and AR40050 to R.L.L. and T32AR0607 to M.A.C.); the National Science Foundation (NSF-Graduate Research Fellowship to M.A.C.); The American Heart Association (12POST12030256 to I.B.); National Key Basic Research Program of China (2013CB531200 to K.O.); and the National Science Foundation of China (31370823 to K.O.).

REFERENCES

1. Lieber, R.L. (2010) *Skeletal Muscle Structure, Function, and Plasticity*, 3rd ed. Lippincott Williams & Wilkins, Philadelphia, PA.
2. Watchko, J.F., O'Day, T.L. and Hoffman, E.P. (2002) Functional characteristics of dystrophic skeletal muscle: insights from animal models. *J. Appl. Physiol.*, **93**, 407–417.
3. Brosig, M., Ferralli, J., Gelman, L., Chiquet, M. and Chiquet-Ehrismann, R. (2010) Interfering with the connection between the nucleus and the cytoskeleton affects nuclear rotation, mechanotransduction and myogenesis. *Int. J. Biochem. Cell Biol.*, **42**, 1717–1728.
4. Houben, F., Ramaekers, F.C.S., Snoeckx, L.H.E.H. and Broers, J.L.V. (2007) Role of nuclear lamina-cytoskeleton interactions in the maintenance of cellular strength. *Biochim. Biophys. Acta*, **1773**, 675–686.
5. Zhang, J., Felder, A., Liu, Y., Guo, L.T., Lange, S., Dalton, N.D., Gu, Y., Peterson, K.L., Mizisin, A.P., Shelton, G.D. *et al.* (2010) Nesprin 1 is critical for nuclear positioning and anchorage. *Hum. Mol. Gen.*, **19**, 329–341.
6. Banerjee, I., Zhang, J., Moore-Morris, T., Pfeiffer, E., Buchholz, K.S., Liu, A., Ouyang, K., Stroud, M.J., Gerace, L., Evans, S.M. *et al.* (2014) Targeted Ablation of Nesprin 1 and Nesprin 2 from murine myocardium results in cardiomyopathy, altered nuclear morphology and inhibition of the biomechanical gene response. *PLoS Genet.*, **10**, e1004114.
7. Shah, S.B., Davis, J., Weisleder, N., Kostavassili, I., McCulloch, A.D., Ralston, E., Capetanaki, Y. and Lieber, R.L. (2004) Structural and functional roles of desmin in mouse skeletal muscle during passive deformation. *Biophys. J.*, **86**, 2993–3008.
8. Stroud, M.J., Banerjee, I., Veevers, J. and Chen, J. (2014) Linker of nucleoskeleton and cytoskeleton complex proteins in cardiac structure, function, and disease. *Circ. Res.*, **114**, 538–548.
9. Bonne, G., Yaou, R.Ben, Béroud, C., Boriani, G., Brown, S., De Visser, M., Duboc, D., Ellis, J., Hausmanowa-Petrusewicz, I., Lattanzi, G. *et al.* (2003) 108th ENMC international workshop, 3rd workshop of the MYO-CLUSTER project: EUROMEN, 7th international emery-dreifuss muscular dystrophy (EDMD) workshop, 13–15 September 2002, Naarden, The Netherlands. *Neuromuscul. Disord.*, **13**, 508–515.
10. Muntoni, F., Bonne, G., Goldfarb, L.G., Mercuri, E., Piercy, R.J., Burke, M., Yaou, R.Ben, Richard, P., Récan, D., Shatunov, A. *et al.* (2006) Disease severity in dominant Emery Dreifuss is increased by mutations in both emerin and desmin proteins. *Brain*, **129**, 1260–1268.
11. Zhang, Q., Bethmann, C., Worth, N.F., Davies, J.D., Wasner, C., Feuer, A., Ragnauth, C.D., Yi, Q., Mellad, J.a., Warren, D.T. *et al.* (2007) Nesprin-1 and -2 are involved in the pathogenesis of Emery Dreifuss muscular dystrophy and are critical for nuclear envelope integrity. *Hum. Mol. Gen.*, **16**, 2816–2833.
12. Meyer, G.A. and Lieber, R.L. (2012) Skeletal muscle fibrosis develops in response to desmin deletion. *Am. J. Physiol. Cell Physiol.*, **302**, C1609–C1620.
13. Warren, D.T., Zhang, Q., Weissberg, P.L. and Shanahan, C.M. (2005) Nesprins: intracellular scaffolds that maintain cell architecture and coordinate cell function? *Expert Rev. Mol. Med.*, **7**, 1–15.
14. Zhang, Q., Ragnauth, C.D., Skepper, J.N., Worth, N.F., Warren, D.T., Roberts, R.G., Weissberg, P.L., Ellis, J.a. and Shanahan, C.M. (2005) Nesprin-2 is a multi-isomeric protein that binds lamin and emerin at the nuclear envelope and forms a subcellular network in skeletal muscle. *J. Cell Sci.*, **118**, 673–687.
15. Simpson, J.G. and Roberts, R.G. (2008) Patterns of evolutionary conservation in the nesprin genes highlight probable functionally important protein domains and isoforms. *Biochem. Soc. Trans.*, **36**, 1359–1367.
16. Rajgor, D., Mellad, J.a., Autore, F., Zhang, Q. and Shanahan, C.M. (2012) Multiple novel nesprin-1 and nesprin-2 variants act as versatile tissue-specific intracellular scaffolds. *PLOS ONE*, **7**, e40098.
17. Zhen, Y.-Y., Libotte, T., Munck, M., Noegel, A.a. and Korenbaum, E. (2002) NUANCE, a giant protein connecting the nucleus and actin cytoskeleton. *J. Cell Sci.*, **115**, 3207–3222.
18. Padmakumar, V.C., Abraham, S., Braune, S., Noegel, A.a., Tunggal, B., Karakesisoglou, I. and Korenbaum, E. (2004) Enaptin, a giant actin-binding protein, is an element of the nuclear membrane and the actin cytoskeleton. *Exp. Cell Res.*, **295**, 330–339.
19. Crisp, M., Liu, Q., Roux, K., Rattner, J.B., Shanahan, C., Burke, B., Stahl, P.D. and Hodzic, D. (2006) Coupling of the nucleus and cytoplasm: role of the LINC complex. *J. Cell Biol.*, **172**, 41–53.
20. Ketema, M. and Sonnenberg, A. (2011) Nesprin-3: a versatile connector between the nucleus and the cytoskeleton. *Biochem. Soc. Trans.*, **39**, 1719–1724.
21. Wilhelmsen, K., Litjens, S.H.M., Kuikman, I., Tshimbalanga, N., Janssen, H., Van den Bout, I., Raymond, K. and Sonnenberg, A. (2005) Nesprin-3, a novel outer nuclear membrane protein, associates with the cytoskeletal linker protein plectin. *J. Cell Biol.*, **171**, 799–810.
22. Milner, D.J., Weitzer, G., Tran, D., Bradley, A. and Capetanaki, Y. (1996) Disruption of muscle architecture and myocardial degeneration in mice lacking desmin. *J. Cell Biol.*, **134**, 1255–1270.
23. Li, Z., Mericskay, M., Agbulut, O., Butler-Browne, G., Carlsson, L., Thornell, L.E., Babinet, C. and Paulin, D. (1997) Desmin is essential for the tensile strength and integrity of myofibrils but not for myogenic commitment, differentiation, and fusion of skeletal muscle. *J. Cell Biol.*, **139**, 129–144.
24. Paulin, D. and Li, Z. (2004) Desmin: a major intermediate filament protein essential for the structural integrity and function of muscle. *Exp. Cell Res.*, **301**, 1–7.

25. Capetanaki, Y., Milner, D.J. and Weitzer, G. (1997) Desmin in muscle formation and maintenance: knockouts and consequences. *Cell Struct. Funct.*, **22**, 103–116.
26. Edwards, C. and O'Brien, W. (1980) Modified assay for determination in a tissue hydrolyzate of hydroxyproline. *Clin. Chim. Acta*, **104**, 161–167.
27. Lange, S., Ouyang, K., Meyer, G., Cui, L., Cheng, H., Lieber, R.L. and Chen, J. (2009) Obscurin determines the architecture of the longitudinal sarcoplasmic reticulum. *J. Cell Sci.*, **122**, 2640–2650.
28. Maison, C. and Almouzni, G. (2004) HP1 and the dynamics of heterochromatin maintenance. *Nat. Rev. Mol. Cell Biol.*, **5**, 296–304.
29. Munari, F., Rezaei-Ghaleh, N., Xiang, S., Fischle, W. and Zweckstetter, M. (2013) Structural plasticity in human heterochromatin protein 1β. *PLOS ONE*, **8**, e60887.
30. Bannister, A.J., Zegerman, P., Partridge, J.F., Miska, E.A., Thomas, J.O., Allshire, R.C. and Kouzarides, T. (2001) Selective recognition of methylated lysine 9 on histone H3 by the HP1 chromo domain. *Nature*, **410**, 120–124.
31. Eberhart, A., Feodorova, Y., Song, C., Wanner, G., Kiseleva, E., Furukawa, T., Kimura, H., Schotta, G., Leonhardt, H., Joffe, B. *et al.* (2013) Epigenetics of eu- and heterochromatin in inverted and conventional nuclei from mouse retina. *Chromosome Res.*, **21**, 535–554.
32. Badugu, R., Yoo, Y., Singh, P.B. and Kellum, R. (2005) Mutations in the heterochromatin protein 1 (HP1) hinge domain affect HP1 protein interactions and chromosomal distribution. *Chromosoma*, **113**, 370–384.
33. Leask, A. and Abraham, D.J. (2004) TGF-beta signaling and the fibrotic response. *FASEB J.*, **18**, 816–827.
34. Last, J.A., King, T.E., Nerlich, A.G. and Reiser, K.M. (1990) Collagen cross-linking in adult patients with acute and chronic fibrotic lung disease: molecular markers for fibrotic collagen. *Am. J. Respir. Crit. Care Med.*, **141**, 307–313.
35. López, B., Querejeta, R., González, A., Larman, M. and Díez, J. (2012) Collagen cross-linking but not collagen amount associates with elevated filling pressures in hypertensive patients with stage C heart failure: potential role of lysyl oxidase. *Hypertension*, **60**, 677–683.
36. Bruusgaard, J.C., Liestøl, K., Ekmark, M., Kollstad, K. and Gundersen, K. (2003) Number and spatial distribution of nuclei in the muscle fibres of normal mice studied in vivo. *J. Physiol.*, **551**, 467–478.
37. Sam, M., Shah, S., Fridén, J., Milner, D.J., Capetanaki, Y. and Lieber, R.L. (2000) Desmin knockout muscles generate lower stress and are less vulnerable to injury compared with wild-type muscles. *Am. J. Physiol. Cell Physiol.*, **279**, C1116–C1122.
38. Friden, J. and Lieber, R.L. (2003) Spastic muscle cells are shorter and stiffer than normal cells. *Muscle Nerve*, **26**, 157–164.
39. Smith, L.R., Fowler-Gerace, L.H., Gerace-Fowler, L. and Lieber, R.L. (2011) Muscle extracellular matrix applies a transverse stress on fibers with axial strain. *J. Biomech.*, **44**, 1618–1620.
40. Zhang, J., Bang, M., Gokhin, D.S., Lu, Y., Cui, L., Li, X., Gu, Y., Dalton, N.D., Scimia, M.C., Peterson, K.L. *et al.* (2008) Syncoilin is required for generating maximum isometric stress in skeletal muscle but dispensable for muscle cytoarchitecture. *Am. J. Physiol. Cell Physiol.*, **0613**, 1175–1182.
41. Banerjee, I., Zhang, J., Moore-Morris, T., Lange, S., Shen, T., Dalton, N.D., Gu, Y., Peterson, K.L., Evans, S.M. and Chen, J. (2012) Thymosin beta 4 is dispensable for murine cardiac development and function. *Circ. Res.*, **110**, 456–464.
42. Shah, S.B. and Lieber, R.L. (2003) Simultaneous imaging and functional assessment of cytoskeletal protein connections in passively loaded single muscle cells. *J. Histochem. Cytochem.*, **51**, 19–29.